# *Coronal Sources and In Situ Properties of the Solar Winds Sampled by ACE During 1999 - 2008*

Fu, Hui; Li, Bo; Li, Xing; Huang, Zhenghua; Mou, Chaozhou; Jiao, Fangran; Xia, Lidong

*Published in:*
Solar Physics

*DOI:*
10.1007/s11207-015-0689-9

*Publication date:*
2015

*Citation for published version (APA):*
Fu, H., Li, B., Li, X., Huang, Z., Mou, C., Jiao, F., & Xia, L. (2015). Coronal Sources and In Situ Properties of the Solar Winds Sampled by ACE During 1999 - 2008. *Solar Physics*, *290*(5), 1399-1415. https://doi.org/10.1007/s11207-015-0689-9

Solar Phys
DOI 10.1007/s11207-015-0689-9

# Coronal Sources and *In Situ* Properties of the Solar Winds Sampled by ACE During 1999 – 2008

**Hui Fu[1] · Bo Li[1] · Xing Li[2] · Zhenghua Huang[1] · Chaozhou Mou[1] · Fangran Jiao[1] · Lidong Xia[1]**

Received: 3 September 2014 / Accepted: 20 April 2015


**Abstract** We identify the coronal sources of the solar winds sampled by the ACE spacecraft during 1999 – 2008 and examine the *in situ* solar wind properties as a function of wind sources. The standard two-step mapping technique is adopted to establish the photospheric footpoints of the magnetic flux tubes along which the ACE winds flow. The footpoints are then placed in the context of EIT 284 Å images and photospheric magnetograms, allowing us to categorize the sources into four groups: coronal holes (CHs), active regions (ARs), the quiet Sun (QS), and "undefined". This practice also enables us to establish the response to solar activity of the fractions occupied by each type of solar wind, and of their speeds and $O^{7+}/O^{6+}$ ratios measured *in situ*. We find that during the maximum phase, the majority of ACE winds originate from ARs. During the declining phase, CHs and ARs are equally important contributors to the ACE solar winds. The QS contribution increases with decreasing solar activity and maximizes in the minimum phase when the QS appears to be the primary supplier of the ACE winds. With decreasing activity, the winds from all sources tend to become cooler, as represented by the increasingly low $O^{7+}/O^{6+}$ ratios. On the other hand, during each activity phase, the AR winds tend to be the slowest and are associated with the highest $O^{7+}/O^{6+}$ ratios, while the CH winds correspond to the other extreme, with the QS winds lying in between. Applying the same analysis method to the slow winds alone, here defined as the winds with speeds lower than 500 km $s^{-1}$, we find basically the same overall behavior, as far as the contributions of individual groups of sources are concerned. This statistical study indicates that QS regions are an important source of the solar wind during the minimum phase.

**Keywords** Solar Wind, sources · Solar wind, properties · Solar cycle

**Electronic supplementary material** The online version of this article (doi:10.1007/s11207-015-0689-9) contains supplementary material, which is available to authorized users.

✉ L. Xia
xld@sdu.edu.cn

[1] Shandong Provincial Key Laboratory of Optical Astronomy and Solar-Terrestrial Environment, Institute of Space Sciences, Shandong University, Weihai, 264209, China

[2] Department of Physics, Aberystwyth University, Aberystwyth, Ceredigion, Wales, UK, SY23 3BZ

Published online: 01 May 2015

## 1. Introduction

Identifying the source regions of the solar wind is important both as a fundamental question in solar physics (Antiochos *et al.*, 2012) and from the space environment perspective (*e.g.*, Luhmann *et al.*, 2002, and references therein). This practice dates back to the era when the solar wind was first measured (Snyder and Neugebauer, 1966; Nolte and Roelof, 1973; Neugebauer *et al.*, 1998, see also Poletto 2013 for a historic overview). With the solar wind data accumulated throughout several solar activity cycles in both near-ecliptic and polar orbits, scenarios have emerged as to how the solar wind sources evolve with solar activity. This concerns not only the solar winds sampled by individual spacecraft, but also the solar winds throughout the heliosphere (Luhmann *et al.*, 2002).

Traditionally, the studies on the solar wind sources start with categorizing the winds into the fast (with proton speeds $v$ over, say, 500 km s$^{-1}$) and slow ones ($v \lesssim 500$ km s$^{-1}$) (*e.g.*, Schwenn, 2006). Regarding the fast solar wind (FSW), the coronal source is generally accepted to be coronal holes (*e.g.*, Krieger, Timothy, and Roelof, 1973; Zirker, 1977; Gosling and Pizzo, 1999). Tracing the wind sampled by *Pioneer VI* and *Vela*, Krieger, Timothy, and Roelof (1973) were the first to associate the FSW with a coronal hole. Then Zirker (1977) suggested that all coronal holes are sources of the FSW. Using the SOHO/SUMER data, the outflows at the base of polar (Hassler *et al.*, 1999) and equatorial (Xia, Marsch, and Curdt, 2003) coronal holes were measured, with the results supporting the notion that the FSW originates in coronal funnels (Tu *et al.*, 2005). On the other hand, while examining the ACE and *Ulysses* data for four Carrington rotations during the Cycle 23 maximum, Neugebauer *et al.* (2002) concluded that a fraction of the FSW also originates from active regions.

The sources of the slow solar wind (SSW) are substantially more complex. While it is consensus that the SSWs are associated with coronal streamers, debates remain as to exactly where in or around streamers the SSWs originate. The scenario proposed for solar minimum conditions by Wang *et al.* (1998) suggests that there are two types of SSWs, with one originating from streamer stalks and the other from just inside coronal holes and immediately adjacent to streamers. The former source is consistent with the outmoving plasmoids found by SOHO/LASCO (Sheeley *et al.*, 1997; Wang *et al.*, 1998), while the latter source is corroborated by the SOHO/UVCS measurements (Abbo *et al.*, 2010) and is consistent with the established inverse correlation of the flow tube expansion with the solar wind speed (Wang and Sheeley, 1990). However, even at solar minimum, this scenario remains to be complemented with the expected source of the SSWs from inside streamers, either through direct flow of the plasma from the magnetically open fields in streamer cores (Noci *et al.*, 1997) or through the evaporation of plasmas from the magnetic arcades in streamer helmets (Suess *et al.*, 1999, also Li *et al.*, 2005). In addition, using the method of interplanetary scintillation (IPS) tomographic analysis, Kojima *et al.* (1999) found that yet another SSW source is the unipolar regions in the vicinity of active regions (ARs). A more direct and detailed study associating the SSW with ARs comes with *Hinode* X-ray and EUV spectral observations, where the edge of ARs was shown to host persistent upflows with speeds reaching 100 km s$^{-1}$ (Harra *et al.*, 2008), which may account for up to one-fourth of the *in situ* SSW (Sakao *et al.*, 2007) provided that these upflows eventually turn into outflows. Indeed, van Driel-Gesztelyi *et al.* (2012) (see also Culhane *et al.*, 2014 and Mandrini *et al.*, 2014) showed that these upflows may access coronal magnetic fields that open into interplanetary space. In addition, using X-ray high temporal-spatial resolution images, Subramanian, Madjarska, and Doyle (2010) found that the magnetic reconnection of co-spatial open and closed magnetic field lines at coronal hole boundaries creates the necessary conditions for plasmas to flow to large distances. This provides an explanation for largely blueshifted events observed

with EIS/*Hinode* (Madjarska *et al.*, 2012), indicating that these plasma outflows are a possible SSW source as well. Comparing the remote sensing and *in situ* measurements, Feldman, Landi, and Schwadron (2005) suggested that the SSW may also arise from the quiet Sun. For solar maximum conditions, SSWs are found to originate from small coronal holes and active regions where open magnetic field lines exist (Neugebauer *et al.*, 2002; Wang and Sheeley, 2003; Liewer, Neugebauer, and Zurbuchen, 2004; Ko *et al.*, 2006; Schwenn, 2006; Wang, Ko, and Grappin, 2009)

While the identified coronal sources of the solar wind are diverse, there seems to be an agreement on the approaches on which the identification procedure is based. First, unlike the solar wind speed itself, ionic charge states, especially those of oxygen and carbon, are suggested to be a telltale signature of the wind sources. Take oxygen, for example. The abundance ratio $O^{7+}/O^{6+}$ measured in the *in situ* solar wind is generally accepted to reflect the electron temperature in the coronal sources, given that it does not vary with distance beyond a fraction of a solar radius above the solar surface (Owocki, Holzer, and Hundhausen, 1983; Büergi and Geiss, 1986; Hefti *et al.*, 2000; Landi *et al.*, 2012b). Because the temperatures are different in different coronal regions, a comparison of the *in situ* charge states allows one to associate the *in situ* wind with a particular coronal source (*e.g.*, Zurbuchen *et al.*, 2000; Zurbuchen, 2001; Landi *et al.*, 2012a). In this spirit, Zhao, Zurbuchen, and Fisk (2009) divided the non-transient solar winds into two categories: those from coronal holes (CH winds) and those from outside coronal holes (non-CH winds) with $O^{7+}/O^{6+}$ values lower and higher than 0.145, respectively. As a result, about 42 % of the ecliptic solar wind was found to be of non-CH origin during 1998 – 2008. Second, a model of coronal magnetic field is often indispensable. For this purpose, while sophisticated magnetohydrodynamic (MHD) models are sometimes adopted (Abbo *et al.*, 2010), the potential-field-source-surface model (PFSS) and its variants have been in much wider use. On the one hand, this practice established that the long-term trend of the wind speed is inversely correlated with the lateral expansion of the flow tubes (Wang and Sheeley, 1990). On the other hand, applying the PFSS model with an archive of the synoptic magnetogram data led Luhmann *et al.* (2002) to the distribution of sources of the heliospheric solar wind as a function of solar activity for nearly three activity cycles. In particular, Luhmann *et al.* (2002) found that although polar coronal holes exist for more than 80 % of a solar cycle, they only contribute to the ecliptic solar winds significantly during half of a cycle. During the other half of a cycle, the near-ecliptic winds instead originate from mid- and low-latitude sources.

Given the diversity of the wind sources and the complexity of the activity-dependence of these sources during a solar activity cycle, the present study is intended to examine, in a statistical manner, the fractions taken up by the *in situ* solar winds from various sources from the activity maximum to minimum in Cycle 23. To this end, we start with the *in situ* wind speed measurements, and adopt the standard two-step mapping procedure (Neugebauer *et al.*, 1998, 2002; Liewer, Neugebauer, and Zurbuchen, 2004) to trace the winds to their footpoints at the solar surface. We then examine the corresponding coronal images recorded by SOHO/EIT as well as photospheric magnetograms, and determine where the footpoints are located: are they located in a coronal hole (CH), an active region (AR), or in the quiet Sun (QS)? The solar winds are therefore grouped accordingly, enabling us to define how their *in situ* properties differ and evolve with different activity levels.

Our study differs from previous studies with similar objectives or similar approaches in the following aspects. First, the approach combining a footpoint-tracing method with the context of coronal images closely follows the approach adopted in Liewer, Neugebauer, and Zurbuchen (2004), which is in turn built on Neugebauer *et al.* (1998, 2002) where the imaging data were not used. However, while Neugebauer *et al.* (1998) focused on the

Cycle 22 – 23 minimum, and Liewer, Neugebauer, and Zurbuchen (2004, also Neugebauer *et al.* 2002) examined the Cycle 23 maximum, we examine the solar wind dataset that spans the interval from 1999 to 2008 in which the declining phase and the Cycle 23 – 24 minimum are included. Furthermore, the solar winds from sources other than CHs and ARs are investigated and are classified as the QS winds. Second, both this study and the one by Zhao, Zurbuchen, and Fisk (2009) (ZZF09 hereafter) have similar objectives in examining the distribution of wind sources in response to solar activity. However, the approach for identifying the sources in this study is different from the one by ZZF09 where the $O^{7+}/O^{6+}$ values are a primary discriminator. We note that, given the uncertainties in both approaches, the results of this study are meant not to be contrasted with but rather to complement ZZF09, with the hope that new light can be shed on the sources of the near-ecliptic solar winds. Third, while both using the PFSS model and being statistical in nature, our study differs from the one by Luhmann *et al.* (2002) in that we also employ the imaging as well as magnetogram data to classify the sources instead of using the locations relative to the equator, as in Luhmann *et al.* (2002). Fourth, given the considerable interest in and the complexities associated with the sources of the slow solar wind, we analyze the ACE solar winds in general and examine the slow ones in particular. In Section 2, we describe the data and our method of analysis. The results are then given in Section 3. Section 4 summarizes the present study, ending with some concluding remarks.

## 2. Data and Analysis

The two-step mapping procedure used in the present study closely follows the one in Neugebauer *et al.* (1998, 2002), Liewer, Neugebauer, and Zurbuchen (2004). To initiate the procedure, we used daily averages of the solar wind speed made with the *Solar Wind Electron, Proton, and Alpha Monitor* (SWEPAM, McComas *et al.*, 1998) onboard the *Advanced Composition Explorer* (ACE, Stone *et al.*, 1998). We also used the daily averages of the abundance ratios $O^{7+}/O^{6+}$ recorded by the *Solar Wind Ion Composition Spectrometer* (SWICS, Gloeckler *et al.*, 1998) and the magnetic field measurements with the *Magnetic Field Experiment* (MAG, Smith *et al.*, 1998). Given that we are interested in the non-transient solar winds, one immediate purpose for using the $O^{7+}/O^{6+}$ ratios is to eliminate from the ACE dataset those intervals occupied by interplanetary *Coronal Mass Ejections* (ICMEs). To do this, we adopted the same approach as in ZZF09 (see also Richardson and Cane, 2004), whereby we discarded the data with $O^{7+}/O^{6+}$ ratios exceeding $6.008\exp(-0.00578v)$, in which $v$ is the wind speed in $\mathrm{km\,s^{-1}}$. A detailed analysis by ZZF09 shows that this criterion adequately separates ICMEs from the non-transient ambient winds, which is reliable in 83.2 % of the cases examined therein. The *in situ* data used in this study span the years between 1999 and 2008, hence encompassing nearly half of Cycle 23.

The mapping procedure involves two steps. First, the loci of the solar winds are found on the source surface, placed at a heliospheric distance of 2.5 $R_\odot$ as implemented by the coronal magnetic field model. This is done in a ballistic approach, whereby the longitude correction due to solar rotation is determined by the time for a wind parcel to travel from the source surface to the spacecraft. Here a constant wind speed was used and assumed to be the one measured by ACE/SWEPAM. The wind parcel is then traced from the source surface to the photosphere by following the magnetic field lines computed by using a PFSS model, provided in the PFSS package as part of the Solar Software. Instead of using the synoptic magnetograms, as was done in *e.g.*, Neugebauer *et al.* (1998), this package uses as the boundary data the magnetograms measured with SOHO/MDI, which are updated every six

**Table 1** Number of daily solar wind samples analyzed in each year.

| Year | All sources | CH winds | AR winds | QS winds | Undefined |
|---|---|---|---|---|---|
| 1999 | 237 (188) | 32 (27) | 148 (117) | 28 (23) | 29 (21) |
| 2000 | 261 (221) | 50 (47) | 145 (125) | 36 (28) | 30 (21) |
| 2001 | 272 (220) | 43 (39) | 155 (119) | 38 (30) | 36 (32) |
| 2002 | 289 (259) | 65 (62) | 152 (135) | 38 (35) | 34 (27) |
| 2003 | 277 (259) | 142 (138) | 71 (65) | 34 (32) | 30 (24) |
| 2004 | 242 (211) | 63 (61) | 94 (81) | 34 (30) | 51 (39) |
| 2005 | 250 (201) | 78 (70) | 70 (61) | 56 (34) | 46 (36) |
| 2006 | 262 (200) | 60 (56) | 55 (43) | 94 (62) | 53 (39) |
| 2007 | 257 (178) | 68 (57) | 36 (30) | 114 (59) | 39 (32) |
| 2008 | 259 (187) | 61 (58) | 29 (27) | 157 (92) | 12 (10) |
| Sum | 2606 (2124) | 662 (615) | 955 (803) | 629 (425) | 360 (281) |

**Table 2** Number of daily slow solar wind samples analyzed in each year.

| Year | All sources | CH winds | AR winds | QS winds | Undefined |
|---|---|---|---|---|---|
| 1999 | 188 (141) | 20 (15) | 119 (89) | 23 (18) | 26 (19) |
| 2000 | 204 (167) | 26 (23) | 123 (103) | 29 (23) | 26 (18) |
| 2001 | 245 (194) | 37 (34) | 139 (103) | 37 (29) | 32 (28) |
| 2002 | 238 (208) | 40 (37) | 135 (118) | 32 (29) | 31 (24) |
| 2003 | 111 (96) | 35 (31) | 36 (32) | 20 (18) | 20 (15) |
| 2004 | 194 (163) | 36 (34) | 83 (70) | 28 (24) | 47 (35) |
| 2005 | 172 (132) | 34 (29) | 52 (44) | 47 (28) | 39 (31) |
| 2006 | 205 (146) | 38 (34) | 40 (28) | 81 (50) | 46 (34) |
| 2007 | 187 (116) | 38 (28) | 30 (25) | 91 (42) | 28 (21) |
| 2008 | 169 (102) | 25 (22) | 15 (13) | 122 (61) | 7 (6) |
| Sum | 1913 (1465) | 329 (287) | 772 (625) | 510 (322) | 302 (231) |

hours. It outputs the magnetic field vector on a $39 \times 384 \times 192$ grid in spherical coordinates inside the source surface (for details, see Schrijver and De Rosa, 2003). It should be noted that as implied by the mapping procedure, the magnetic polarity at the field line footpoint needs to be checked against the one measured *in situ*. Schrijver and De Rosa (2003) found that during 1997 – 2001, 83 % of footpoint polarities matched the interplanetary magnetic field (IMF) measurements at Earth. In this work, we find a similar behavior: the footpoint polarities are consistent with what is measured by ACE/MAG in 81 % of the data from 1999 to 2008. To ensure consistency, we did not include in our further analysis dates for which the polarities at the two ends of the mapping procedure do not match. Table 1 presents the number of daily samples of the non-transient solar wind (second column, labeled "All sources") as a function of time, which is subdivided into the counts of the solar winds from CHs (third column), ARs (fourth), QS (fifth), and Undefined sources (sixth). Given in the parentheses are the numbers that correspond to the cases where the magnetic polarities match. In total, 2124 samples are examined for 1999 – 2008 in our further analysis, of which 615 (803, 425) samples are associated with CHs (ARs, the QS). There is a significant mismatch in 2007 and 2008. This might be explained by the closeness of the ACE spacecraft to the heliospheric current sheet at the cycle minimum. When mapping the winds to the source surface, a small uncertainty may lead to an incorrect polarity. For future reference, Table 2 presents the com-

parison between the footpoint and the *in situ* polarity for the slow solar winds with speeds lower than 500 km $s^{-1}$.

The footpoints were then placed in the context of photospheric magnetograms and the EUV images taken by the *Extreme ultraviolet Imaging Telescope* (EIT, Delaboudinière *et al.*, 1995) onboard SOHO (*Solar and Heliospheric Observatory*, Domingo, Fleck, and Poland, 1995). While EIT operates at a number of passbands (Fe IX/X 171 Å, Fe XII 195 Å, Fe XV 284 Å, and He II 304 Å), we chose the 284 Å passband because the images recorded there reflect the corona at the highest altitude, such that coronal holes are more visible. In this passband, EIT took full-Sun images with a pixel size of 2.6″ four times a day. For consistency, the field line footpoints were compared with images taken at around 13:00 UT on the day corrected for the wind travel time.

The classification scheme is illustrated in Figure 1, where the EIT images (the left column) are overplotted with the footpoint locations represented by the red crosses. The photospheric magnetograms, on which our scheme also relies, were derived from the PFSS model and are given in the right column. The scheme is detailed as follows.

A quantitative approach for identifying coronal hole boundaries is implemented, and the winds that have footpoints located within these identified coronal holes (CHs) are classified as "CH winds" accordingly. This approach, which largely follows that in Krista and Gallagher (2009) and Ko *et al.* (2014), is illustrated in Figure 2. If a footpoint is located inside or close to an apparently dark area, then a rectangular box (the white box in Figure 2a) is chosen to enclose this part of the dark region and its surrounding area. An intensity histogram is constructed, and a multipeak distribution is then obvious (Figure 2c). The well-defined minimum between the first two peaks then defines the threshold for identifying the CH boundary (see the contours in Figure 2a, also Figure 2b, which is the enlarged version of the part inside the box). On the one hand, this scheme enables objectively defining CH boundaries using the EUV images in only one passband; on the other hand, it is not influenced by the variation of coronal emissions with solar activity.

A description of some technical details for implementing this scheme seems necessary. In practice, we started with determining whether there is a dark region close to the traced-back footpoint. By "close", we mean roughly "within 100 arcsecs". If this is the case, we drew a rectangular box, varying in size, but typically a few hundred arcsecs across, that enclosed both a substantial part of the dark region and its surrounding area. The footpoint was always within this box. We found that as long as the box is sufficiently large, its size does not significantly influence what one identifies as CH boundaries because the minima in the different histograms pertinent to different box sizes do not differ substantially. If the dark region is not close to the footpoint, we visually chose the dark area that is the closest to the footpoint and used the same approach to delineate the CH boundary (see *e.g.*, Figure 1d1). If there is no large apparent EUV CH altogether, then we used the threshold found for some obvious CHs one or a few days before this particular day (an example is shown in Figure 1b1, where the CHs near the two poles are contaminated so significantly that the minimum between the first two peaks in the intensity histogram can hardly be discerned). The box is substantially smaller than the disk size, but we nonetheless used the threshold to delineate CH boundaries throughout the entire solar disk. A location-dependent threshold may be more accurate for mapping CH boundaries on the entire disk, but our approach suffices, given that our purpose is to examine whether the footpoint is located inside a CH. In addition, as illustrated by Figure 2a, while a single threshold is adopted, the contours outside the box (the dotted lines) also outline CHs rather accurately.

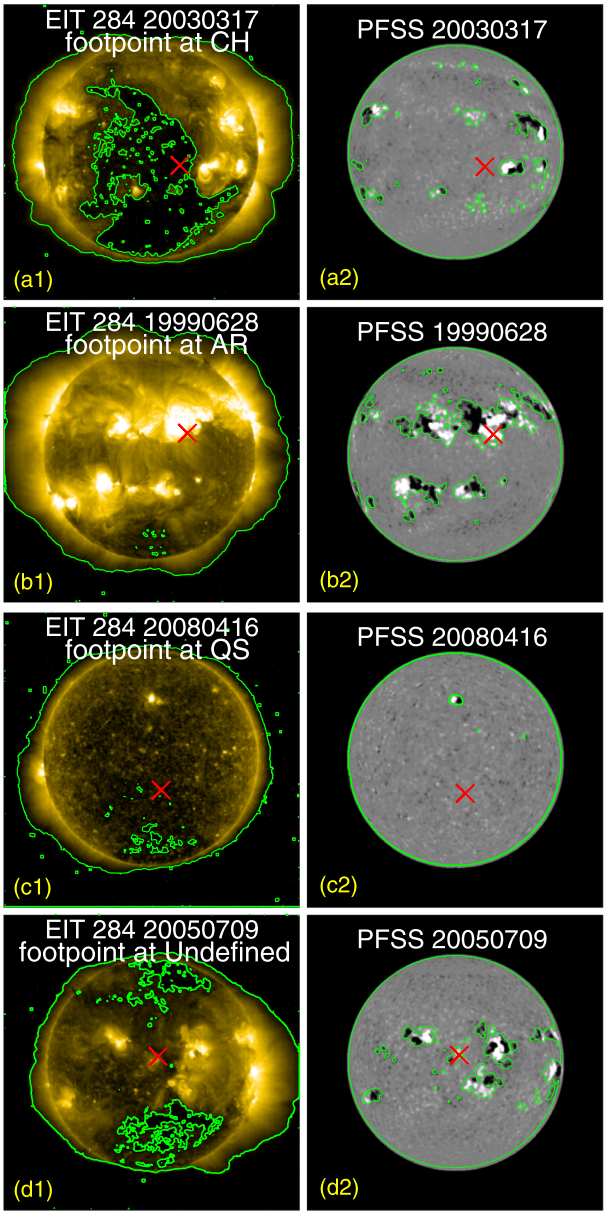


**Figure 1** Illustration of the classification scheme of the ACE solar winds. The footpoints of the solar wind flow tubes are indicated by the red crosses. The footpoints are classified as being associated with a coronal hole (the first row), an active region (second), the quiet Sun (third), and some undefined source (bottom). The left column presents the EIT 284 Å images, while the right column gives the corresponding magnetic morphology of the photosphere. The green contours outline CH (left column) and magnetically concentrated area (MCA) boundaries (right). An animation showing the sources during 1999 – 2008 is available online (see electronic supplementary material).

Our association of a footpoint with an active region (AR) or the quiet Sun (QS) relies on the magnetic morphology of the photospheric regions embodying the identified footpoints. The most obvious features in the photosphere are magnetic clusters, which are tentatively named "magnetically concentrated area" (MCA). Intuitively speaking, MCAs correspond to strong magnetic fields. To make this definition more objective, the absolute value of the radial component of the photospheric magnetic field $|B_{r,\odot}|$ computed from the PFSS model was used. We experimented with different contour levels, $|B_{r,\odot}|_B$, used for outlining MCAs

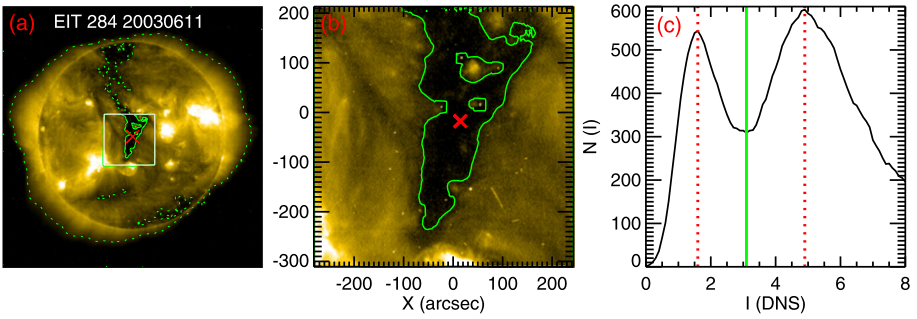


**Figure 2** The scheme for outlining coronal holes. Panel (a) presents the EIT 284 image on 2003 June 11, when the traced-back footpoint (the red cross) is located within a low-latitude CH. The white box encloses the region for which the intensity histogram is constructed and presented in panel (c), where the solid green line represents the minimum between the two peaks, given by the two red dotted lines. This minimum is used as the threshold to delineate CH boundaries in (a), where the contours inside (outside) the box are given by the solid (dotted) lines. Panel (b) is an enlarged version of the part enclosed by the box in (a).

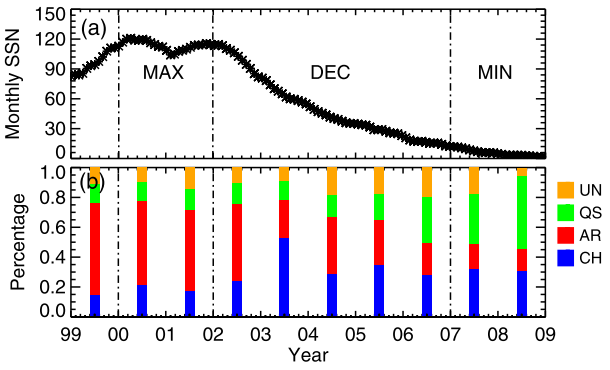


**Figure 3** Fractions of the ACE winds with different sources as a function of time. Panel (a) shows the temporal evolution of the smoothed monthly sunspot number during 1999 – 2008, which is further divided into the maximum (labeled MAX), declining (DEC), and minimum (MIN) phases. Panel (b) gives the percentage of the coronal hole (CH, blue), active region (AR, red), quiet Sun (QS, green), and undefined (UN, orange) winds.

presented in Figure 1 and the attached movie. In practice, if $|B_{r,\odot}|_B$ is assigned a value 1.5 – 4 times the mean of $|B_{r,\odot}|$, then MCAs become well defined. That the MCA morphology is not sensitive to some given $|B_{r,\odot}|_B$, as long as it is in the mentioned range, suggests that MCAs have sharp boundaries. This is understandable considering that MCAs have a strong spatial gradient in $|B_{r,\odot}|$. The thus-defined MCAs encompass all the active regions numbered by NOAA as provided by solarmonitor.[1] However, not all MCA patches correspond to a numbered AR. Many of these correspond to plages with a magnetic field weaker than concurrent numbered ARs (see Section 3.2 in Zharkova *et al.* 2005). In the three solar activity phases (solar maximum, declining phase, and minimum, see Figure 3), the contour levels are chosen to be 2.0, 2.5, and 3.0 times the mean of $|B_{r,\odot}|$, respectively. In the MAX and DEC phases, the threshold is about 10 – 20 G, which is close to the lower bound (15 G) adopted by Wang, Ko, and Grappin (2009) to identify slow solar winds originating from ARs.

With CH boundaries quantitatively defined, we need only to consider the regions outside CHs when we identify AR and QS sources. An AR source is defined when a footpoint is located inside an MCA that is a numbered AR by NOAA. Likewise, QS sources are defined when a footpoint is located outside any MCA.

[1] http://solarmonitor.org.

The sources that are not classified in this grouping scheme are then named "undefined", and they correspond to the case where a footpoint is inside some MCA that is not numbered by NOAA. These sources may be associated with a decaying or developing AR, but it is also possible that they are distinct from AR sources (see, *e.g.*, 06/25 – 06/27 2005 in the movie where the source is likely a QS region). This is why we chose to call them "undefined'.

This scheme does not overestimate the counts in the respective groups. First, the counts of AR and QS sources are not overestimated, since some footpoints deemed "undefined" may in fact be AR and QS sources. Second, the counts of CH winds are not overestimated either because the current definition of CHs excludes a fraction of CHs with overlying and foreground bright emissions. In any case, the counts in the undefined group account for only a minor fraction of the samples (11.2 %, 9.5 %, 14.5 %, 10.4 %, 9.3 %, 18.5 %, 17.9 %, 19.5 %, 18.0 %, and 5.3 % for the years 1999 to 2008, respectively).

Before proceeding, several remarks on our approach seem in order. The first remark is on the reliability of the PFSS model, given its apparent oversimplification of imposing a spherical source surface, neglecting volumetric electric currents between the source surface and the photosphere, and assuming purely radially directed field lines outside the source surface. Nonetheless, a detailed comparison study by Riley *et al.* (2006) demonstrated that the magnetic field configuration computed by the simple PFSS model agrees well with the configuration found in sophisticated MHD simulations, provided that both models are driven by the same line-of-sight magnetograms. From the practical point of view, the magnetically open regions obtained by the PFSS model match the coronal hole regions that were identified for instance in the He I 10830 synotpic diagrams (Levine, 1982; Neugebauer *et al.*, 1998, 2002; Schrijver and De Rosa, 2003). A good way to ensure that the traced-back footpoints are reasonably accurate is to compare the current SolarSoft PFSS results with some other calculations. To address this, we randomly chose three Carrington rotations in the MAX, DEC, and MIN phases, and compared our derived footpoints with those derived from the PFSS model where the magnetogram input is taken from the Wilcox Solar Observatory (WSO). We found that the fraction of the days when the two different sets of footpoints belong to the same open field region is 80.7 % for CR 1969, 84 % for CR 2005, and 82.6 % for CR 2054. Nevertheless, we stress that the fraction at which the two sets do agree is substantial enough that the statistical study we conduct can be deemed reliable.

Another source of uncertainty may come from the mapping procedure, particularly in view of the simple ballistic treatment involved in the first step. As demonstrated by Nolte and Roelof (1973) (also see Neugebauer *et al.*, 2002), while the solar wind may experience some acceleration beyond the source surface, this effect may be counter-balanced by the near-Sun corotation. Another piece of evidence lending us confidence with this mapping procedure is that inspecting the footpoints on a consecutive basis (see online animation 1 in electronic supplementary material) shows an orderly distribution of the footpoint locations. They stay in a particular group for several days before moving to another group. In addition, assuming that the uncertainty with the source longitude at the source surface is $\pm 10^{\circ}$ (Nolte and Roelof, 1973), we selected two Carrington rotations in each subinterval (see Figure 3a) and examined how well our classification scheme works. This was done by tracing the photospheric footpoint from a locus on the source surface 10° eastward or westward of the nominal locus, and then examining whether the footpoint is located in a different area in the EIT images. We found that at maximum activity, about 30 % of the footpoints are associated with an area different from what we identified using the nominal locus. During the declining and minimum phases, however, this mismatch reduces to $\lesssim 20$ % and 10 % of the cases examined, respectively.

## 3. Results

### 3.1. Sources of the ACE Wind Between 1999 and 2008

After categorizing the winds, we defined the percentage of each type of wind and how this evolves in response to solar activity. Figure 3a presents the monthly average of the smoothed sunspot numbers from 1999 to 2008. Three subintervals, labeled MAX, DEC, and MIN, were defined according to the level of solar activity. Figure 3b presents the percentage of the CH (shaded blue), AR (red), QS (green), and undefined (orange) winds in this period. These percentages are yearly averaged values and add up to unity in each year. In the subinterval MAX, the QS supplies only a small fraction of the winds sampled by ACE ($\sim 10$ %), the contributions from CHs is $\sim 15-20$ %, and more than half (56 %) of the ACE winds originates from ARs. In the declining phase (2002 – 2006), the contributions from CHs and ARs both amount to roughly 34 %, and the contributions from ARs (QS) tend to decrease (increase). For the subinterval MIN (2007 – 2008), the fraction of the winds from ARs is very small ($\lesssim 17$ %), while some 31 % comes from the CHs, and nearly half of the winds originates from the QS.

Despite the differences in the approaches for identifying the solar wind sources, Figure 3 agrees with Figure 1 in ZZF09 in that there exists a tendency for coronal sources other than CHs to contribute significantly to the ACE solar winds between 1999 and 2008. Overall, Figure 3b indicates that non-CH sources may be more important than CHs in terms of their mass supply to the solar wind. In particular, Figure 3b indicates that the majority of the near-Earth solar wind comes from ARs during the Cycle 23 maximum. This behavior agrees with ZZF09 and seems to persist to the Cycle 24 maximum, as indicated by the very recent study by Brooks, Ugarte-Urra, and Warren (2015). Furthermore, Figure 3 indicates that CH winds tend to dominate in the year of 2003, which is also in line with ZZF09. Figure 3 is new in that it combines the imaging and the magnetogram data, which allows us to further determine, among the sources outside CHs, the fractions of the winds from ARs and the QS. Some apparent differences from ZZF09 arise as a result. Around the Cycle 23 – 24 minimum, while ZZF09 indicated that CH winds dominate, our Figure 3b suggests that the contribution from the QS is more important. We stress that this apparent discrepancy stems from the differences in the schemes for classifying the solar winds.

More insights can be gained by examining how the *in situ* properties of the solar winds categorized by our scheme depend on solar activity. We sorted the wind speeds $v$ into six bins uniformly spaced between 200 and 800 km s$^{-1}$, grouped the $O^{7+}/O^{6+}$ ratios into six bins uniformly spaced between 0.0 and 0.6, and present in Figure 4 a contour plot in the $v$–$O^{7+}/O^{6+}$ space the counts of the winds from different sources as labeled. The left, middle, and right columns correspond to the intervals MAX, DEC, and MIN, respectively. We first consider the interval MAX (left column). The majority of the winds corresponds to an $O^{7+}/O^{6+}$ ratio higher than 0.145, which we recall is the criterion that ZZF09 employed to separate CH winds from non-CH ones. However, a more detailed analysis like ours indicates that not all winds that have $O^{7+}/O^{6+}$ ratios lower than the nominal value of 0.145 are from CHs. Conversely, winds with $O^{7+}/O^{6+}$ exceeding 0.145 are not necessarily non-CH winds. The years 2007 and 2008, labeled MIN, are considered next. Figure 4 (right column) shows that the $O^{7+}/O^{6+}$ ratios tend to be low, with the majority being lower than 0.145, meaning that if the ACE winds are categorized by this threshold, one would find that nearly all the winds are from CHs. However, combining the footpoint-tracing approach with the EUV and magnetic field data, we find that the QS is the primary contributor to the ACE winds during this period. Furthermore, comparing Figures 4c1 with 4c3, the QS winds are distinct from

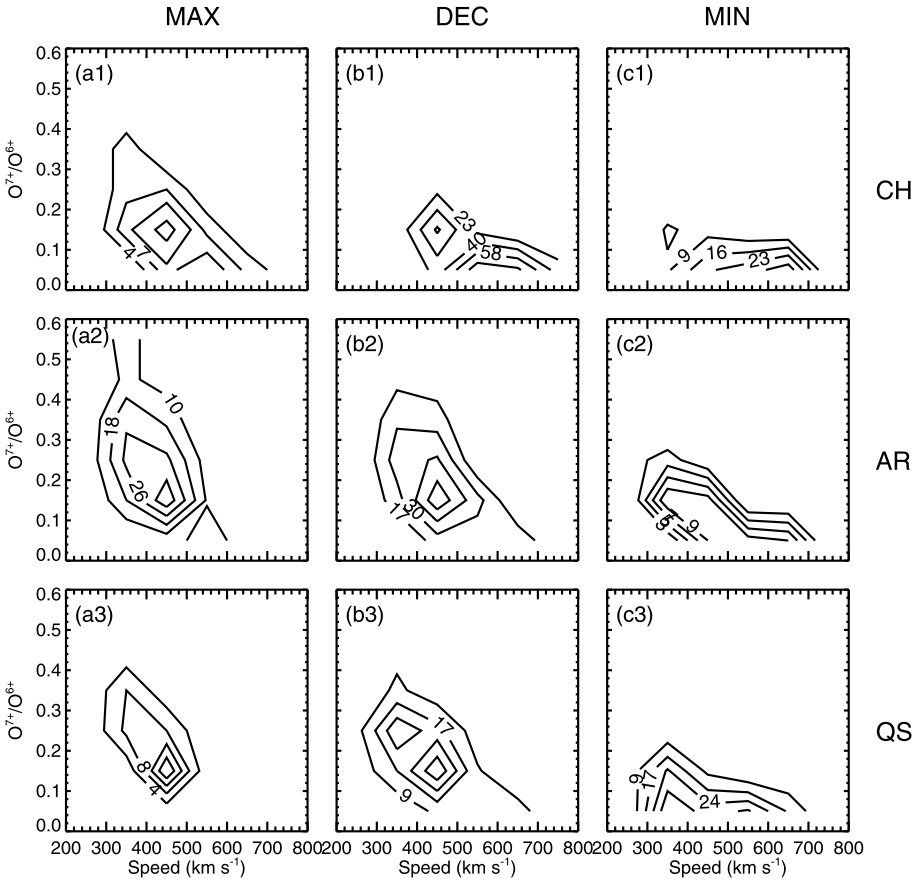


**Figure 4** Dependence on solar activity of the distribution of solar winds from different sources in the speed–$O^{7+}/O^{6+}$ space. The left (middle, right) column corresponds to the maximum (declining, minimum) phase, while the first (second, third) row represents the winds from coronal holes (active regions, the quiet Sun). Here the counts of solar wind samples in different groups are shown as contour plots with the contours equally spaced in each panel.

the CH winds in that they tend to be substantially slower. To select the proper subset of the fast solar wind sampled by ACE that comes from CHs, there can be almost no doubt in choosing those with speeds higher than 600 km $s^{-1}$ and $O^{7+}/O^{6+}$ lower than 0.05, for instance. The contamination from the QS winds would be at most marginal, and that from the AR winds would be minimal. We note in passing that this practice has been successfully employed by Zhao and Landi (2014). In the declining phase (middle column of Figure 4) the possibility of distinguishing between CH winds and non-CH winds lies in between the extremes of MAX and MIN conditions. This is particularly true in the speed dimension. The CH winds tend to be faster than the non-CH winds (mainly from ARs in this case), and the difference between them tends to be more obvious than for the MAX phase, but appears significantly less obvious than for the MIN phase.

The $O^{7+}/O^{6+}$ ratios for the CH winds during the MAX phase (Figure 4a1) require some explanation. There appears to be a fraction of the CH winds for which the $O^{7+}/O^{6+}$ values exceed 0.26. If assuming ionization equilibrium, this would correspond to a freeze-in

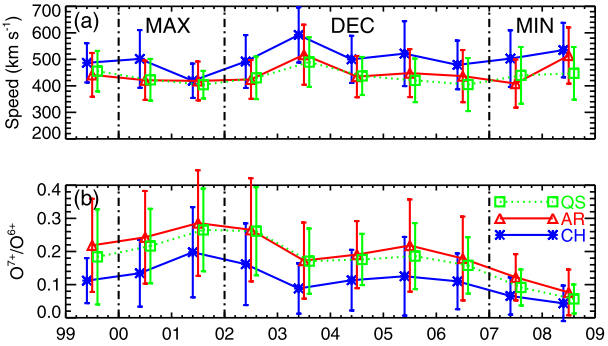


**Figure 5** *In situ* properties of solar winds from different sources as a function of time during 1999 – 2008. Here panels (a) and (b) are for the wind speeds and $O^{7+}/O^{6+}$ ratios, respectively. The interval between 2000 and 2008 is further divided into three activity phases: maximum (MAX), declining (DEC), and minimum (MIN). The winds from coronal holes (CHs), active regions (ARs), and the quiet Sun (QS) are represented by the blue, red, and green curves, respectively. The error bars represent the standard deviations in each year.

temperature exceeding 1.58 MK (Mazzotta *et al.*, 1998). This is beyond the currently accepted electron temperatures derived from remote-sensing measurements for CHs below 1.6 $R_\odot$ (Habbal, Esser, and Arndt, 1993; Esser and Edgar, 2000 and references therein). This apparent discrepancy is of little effect given that this fraction of the CH winds tends to originate from the boundaries between CHs and ARs, while the measurements made by Habbal, Esser, and Arndt (1993) pertain to the region well inside a polar CH. Furthermore, as proposed by Esser and Edgar (2000), the electron distribution function may rapidly develop a non-Maxwellian character within the first several solar radii that eventually forms what is measured *in situ* as the halo electrons (Marsch, 2006). It is worth noting that this non-Maxwellian character is also possible to develop in AR and QS winds.

The differences in the *in situ* properties of the winds from different sources are examined in more detail in Figure 5, where (a) the wind speed and (b) the oxygen charge state ratio are plotted as a function of time. Given by the green, red, and blue curves are the parameters of the QS, AR, and CH winds, respectively. The standard deviations are given by the error bars for the corresponding values, which are slightly displaced from one another for display purposes. An immediate impression from Figure 5 is that the CH winds tend to be the fastest, while the AR and QS winds have almost equal speeds. The $O^{7+}/O^{6+}$ ratios are lowest (highest) for CH (AR) winds, with the QS winds lying in between. However, the considerable overlap in either the speed or $O^{7+}/O^{6+}$ ranges means that neither of the two parameters, on its own, seems to suffice to distinguish the wind sources. For the activity-dependence of the parameters, Figure 5a shows that the wind speeds in the three categories display a similar non-monotonic behavior. The speed of the CH winds, for instance, starts from relatively low values ($\sim 500$ km s$^{-1}$) around MAX and rises to some 590 km s$^{-1}$ in 2003 before decreasing to around 500 km s$^{-1}$ in 2004 – 2006, and then gradually increases to some 550 km s$^{-1}$ toward the MIN phase. Figure 5b shows that the overall tendency of $O^{7+}/O^{6+}$ ratios in response to solar activity is opposite to that of the speed, as would be expected given the well-established inverse correlation of the two parameters (Wang and Sheeley, 2003; Wang, Ko, and Grappin, 2009). Nonetheless, one can see that the $O^{7+}/O^{6+}$ ratios from different groups of winds differ more significantly than the speeds do: Note the marked difference in the $O^{7+}/O^{6+}$ values in the CH winds from those in the AR winds in the whole period. It is noteworthy that with decreasing activity, the $O^{7+}/O^{6+}$ ratios in all three types of solar winds tend to decrease, which agrees with Lepri, Landi, and Zurbuchen

(2013). The $O^{7+}/O^{6+}$ values in AR (CH) winds are 0.26 (0.16) during MAX and decrease to 0.10 (0.05) during MIN.

### 3.2. Sources of the ACE Slow Wind Between 1999 and 2008

Given the considerable interest in understanding the origins of the slow solar wind (SSW), it is informative to apply the same practice to the slow winds alone. In the present study, an SSW is defined to be the wind with speeds lower than 500 km s$^{-1}$. Figure 6 examines the time evolution of the fractions of the SSWs coming from various sources during 1999 – 2008. Overall, the impression in the MAX and DEC phases is similar to what one finds in Figure 3, where the solar winds as a whole were considered. This similarity to Figure 3b is not surprising given that, as shown in Figure 4, most of the solar winds is on the lower side when the speed is concerned. During the MIN phase, the contribution from the QS to the slow wind is even more important than that to the overall solar wind. This is also understandable in view of Figure 4c1, given that the solar winds from CHs are largely fast ones.

Figure 7 presents (a) the wind speeds and (b) the $O^{7+}/O^{6+}$ ratios for the slow solar wind as a function of time. The wind speeds in a given group do not show a systematic variation with solar activity. In addition, there is no clear-cut difference in the speeds of the winds from different groups. A stronger temporal variation and a more significant difference in different groups of winds lie in the $O^{7+}/O^{6+}$ values (Figure 7b). Overall, the $O^{7+}/O^{6+}$ values for all the winds show a decrease with decreasing solar activity, and they are substantially different for different groups. The differences in the $O^{7+}/O^{6+}$ values in winds from different sources may be a result of the intrinsic difference in the respective source properties, the magnetic field strength being the most likely one. This reinforces the notion raised by Antiochos *et al.* (2012), who suggested that the compositional properties and temporal variability serve better in differentiating the wind sources than the speeds.

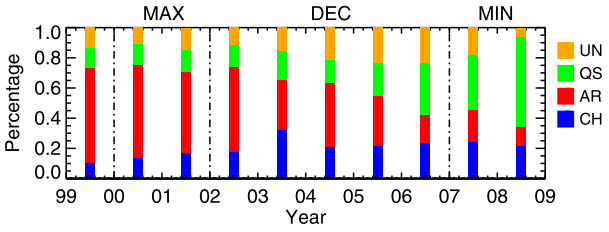


**Figure 6** Similar to Figure 3, but restricted to the slow wind with speeds lower than 500 km s$^{-1}$.

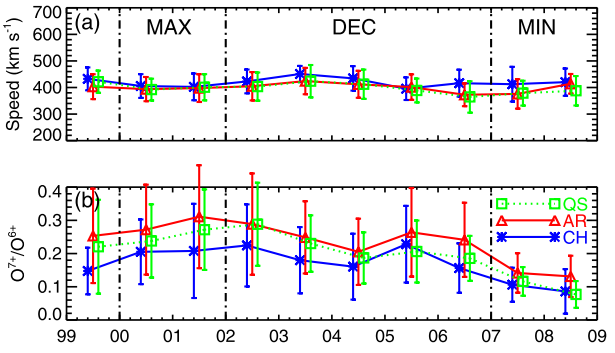


**Figure 7** Similar to Figure 5, but restricted to the slow wind.

The SSW properties may be compared with previous studies. Wang, Ko, and Grappin (2009) suggested that the slow wind during 1998 – 2007 mainly contains two components: one from small holes located in and around ARs with high $O^{7+}/O^{6+}$ ratios during maximum, the other from the boundaries of large CHs with intermediate $O^{7+}/O^{6+}$ values. Our approach suggests that the majority of the former component indeed comes from ARs during maximum. However, the latter component may actually come from all the three kinds of sources (see Figure 4).

## 4. Conclusions

The main purpose of this work was to examine in a statistical sense the sources of the solar wind sampled by ACE during 1999 – 2008 in general and those of the slow solar wind in particular. To this end, we started with the *in situ* wind speed and found the photospheric footpoints of the wind parcels by employing the standard two-step mapping procedure (Neugebauer *et al.*, 1998, 2002) where the Potential Field Source Surface (PFSS) model (Schatten, Wilcox, and Ness, 1969; Altschuler and Newkirk, 1969) was used. We then associated the footpoints with various areas in the EUV images recorded by EIT in its 284 Å passband and photospheric magnetograms. With this association, we classified the ACE winds into three groups: coronal hole (CH), active region (AR), and quite-Sun (QS) winds. Our main results can be summarized as follows.

i) During the Cycle 23 maximum (years 2000 and 2001), ARs are the main contributor to the ACE winds, the contribution of CHs (QS) is $\sim 20$ % (13 %). The winds in this interval tend to be slow, and the AR winds correspond to substantially higher $O^{7+}/O^{6+}$ values than the CH winds. During the declining phase, the contributions from CHs and ARs both amount to roughly one third. Overall, the fraction of the QS winds in this period is 17 % and tends to increase with decreasing activity, accounting for 31 % of the winds in 2006. During the Cycle 23 – 24 minimum (2007 and 2008), the contribution of CHs (ARs) is about 31 % (15 %), while the QS contribution is $\sim 41$ %.
ii) Overall, in each phase of solar activity, the winds from CHs tend to be the fastest and associated with the lowest $O^{7+}/O^{6+}$ ratios. While both are lower than CH winds, the speeds of AR and QS winds do not show a substantial difference. A slightly more pronounced difference between AR and QS winds is seen in their $O^{7+}/O^{6+}$ values, with AR winds tending to be slightly hotter. With decreasing activity, the winds generally tend to have lower $O^{7+}/O^{6+}$ ratios.
iii) The fractions occupied by the slow solar winds from different groups show a dependence on solar activity similar to the case where solar winds from all speed ranges are considered. This can also be said for the activity dependence of $O^{7+}/O^{6+}$ values. During the minimum phase, the QS contribution to the slow wind is even more important than its overall contribution, amounting to $\sim 47$ %.

Our results suggest that the quiet Sun is an important source of the ACE solar winds around the Cycle 23 – 24 minimum. A more detailed study dedicated to examining the properties of the source region and *in situ* properties of this particular QS wind is needed. Properties such as the magnetic field strength and magnetic topology will be of interest for the source regions. For *in situ* properties, the abundances of low first-ionization-potential elements relative to their photospheric values will be informative (Feldman, Landi, and Schwadron, 2005; Wang, Ko, and Grappin, 2009). In addition, it will be worthwhile to search for direct signatures of outflow in the QS by examining the Doppler shifts with the

emission lines measured with either SOHO/SUMER (*e.g.*, Xia, Marsch, and Curdt, 2003) or *Hinode*/EIS (*e.g.*, Fu *et al.*, 2014; Brooks, Ugarte-Urra, and Warren, 2015).

**Acknowledgements** We would like to thank the anonymous referee for helpful comments. We thank the ACE SWICS, SWEPAM, and MAG instrument teams and the ACE Science Center for providing the ACE data. SOHO is a project of international cooperation between ESA and NASA. Wilcox Solar Observatory data used in this study were obtained via the web site http://wso.stanford.edu courtesy of J.T. Hoeksema. The Wilcox Solar Observatory is currently supported by NASA. This research is supported by the China 973 program 2012CB825601, the National Natural Science Foundation of China (41174154, 41274176, and 41274178), and the Ministry of Education of China (20110131110058 and NCET-11-0305). BL is also grateful to the International Space Science Institute (ISSI) for providing the financial support to the international team on the origins of the slow solar wind.

## References

Abbo, L., Antonucci, E., Mikić, Z., Linker, J.A., Riley, P., Lionello, R.: 2010, Characterization of the slow wind in the outer corona. *Adv. Space Res.* **46**, 1400. DOI. ADS.

Altschuler, M.D., Newkirk, G.: 1969, Magnetic fields and the structure of the solar corona. I: Methods of calculating coronal fields. *Solar Phys.* **9**, 131. DOI. ADS.

Antiochos, S.K., Linker, J.A., Lionello, R., Mikić, Z., Titov, V., Zurbuchen, T.H.: 2012, The structure and dynamics of the corona–heliosphere connection. *Space Sci. Rev.* **172**, 169. DOI. ADS.

Brooks, D.H., Ugarte-Urra, I., Warren, H.P.: 2015, Full-Sun observations for identifying the source of the slow solar wind. *Nat. Commun.* **6**, 5947. DOI. ADS.

Büergi, A., Geiss, J.: 1986, Helium and minor ions in the corona and solar wind – dynamics and charge states. *Solar Phys.* **103**, 347. DOI. ADS.

Culhane, J.L., Brooks, D.H., van Driel-Gesztelyi, L., Démoulin, P., Baker, D., DeRosa, M.L., Mandrini, C.H., Zhao, L., Zurbuchen, T.H.: 2014, Tracking solar active region outflow plasma from its source to the near-Earth environment. *Solar Phys.* **289**, 3799. DOI. ADS.

Delaboudinière, J.-P., Artzner, G.E., Brunaud, J., Gabriel, A.H., Hochedez, J.F., Millier, F., Song, X.Y., Au, B., Dere, K.P., Howard, R.A., Kreplin, R., Michels, D.J., Moses, J.D., Defise, J.M., Jamar, C., Rochus, P., Chauvineau, J.P., Marioge, J.P., Catura, R.C., Lemen, J.R., Shing, L., Stern, R.A., Gurman, J.B., Neupert, W.M., Maucherat, A., Clette, F., Cugnon, P., van Dessel, E.L.: 1995, EIT: extreme-ultraviolet imaging telescope for the SOHO mission. *Solar Phys.* **162**, 291. DOI. ADS.

Domingo, V., Fleck, B., Poland, A.I.: 1995, The SOHO mission: an overview. *Solar Phys.* **162**, 1. DOI. ADS.

Esser, R., Edgar, R.J.: 2000, Reconciling spectroscopic electron temperature measurements in the solar corona with in situ charge state observations. *Astrophys. J. Lett.* **532**, L71. DOI. ADS.

Feldman, U., Landi, E., Schwadron, N.A.: 2005, On the sources of fast and slow solar wind. *J. Geophys. Res.* **110**, 7109. DOI. ADS.

Fu, H., Xia, L., Li, B., Huang, Z., Jiao, F., Mou, C.: 2014, Measurements of outflow velocities in on-disk plumes from EIS/Hinode observations. *Astrophys. J.* **794**, 109. DOI. ADS.

Gloeckler, G., Cain, J., Ipavich, F.M., Tums, E.O., Bedini, P., Fisk, L.A., Zurbuchen, T.H., Bochsler, P., Fischer, J., Wimmer-Schweingruber, R.F., Geiss, J., Kallenbach, R.: 1998, Investigation of the composition of solar and interstellar matter using solar wind and pickup ion measurements with SWICS and SWIMS on the ACE spacecraft. *Space Sci. Rev.* **86**, 497. DOI. ADS.

Gosling, J.T., Pizzo, V.J.: 1999, Formation and evolution of corotating interaction regions and their three dimensional structure. *Space Sci. Rev.* **89**, 21. DOI. ADS.

Habbal, S.R., Esser, R., Arndt, M.B.: 1993, How reliable are coronal hole temperatures deduced from observations? *Astrophys. J.* **413**, 435. DOI. ADS.

Harra, L.K., Sakao, T., Mandrini, C.H., Hara, H., Imada, S., Young, P.R., van Driel-Gesztelyi, L., Baker, D.: 2008, Outflows at the edges of active regions: contribution to solar wind formation? *Astrophys. J. Lett.* **676**, L147. DOI. ADS.

Hassler, D.M., Dammasch, I.E., Lemaire, P., Brekke, P., Curdt, W., Mason, H.E., Vial, J.-C., Wilhelm, K.: 1999, Solar wind outflow and the chromospheric magnetic network. *Science* **283**, 810. DOI. ADS.

Hefti, S., Grünwaldt, H., Bochsler, P., Aellig, M.R.: 2000, Oxygen freeze-in temperatures measured with SOHO/CELIAS/CTOF. *J. Geophys. Res.* **105**, 10527. DOI. ADS.

Ko, Y.-K., Raymond, J.C., Zurbuchen, T.H., Riley, P., Raines, J.M., Strachan, L.: 2006, Abundance variation at the vicinity of an active region and the coronal origin of the slow solar wind. *Astrophys. J.* **646**, 1275. DOI. ADS.

Ko, Y.-K., Muglach, K., Wang, Y.-M., Young, P.R., Lepri, S.T.: 2014, Temporal evolution of solar wind ion composition and their source coronal holes during the declining phase of cycle 23. I. Low-latitude extension of polar coronal holes. *Astrophys. J.* **787**, 121. DOI. ADS.

Kojima, M., Fujiki, K., Ohmi, T., Tokumaru, M., Yokobe, A., Hakamada, K.: 1999, Low-speed solar wind from the vicinity of solar active regions. *J. Geophys. Res.* **104**, 16993. DOI. ADS.

Krieger, A.S., Timothy, A.F., Roelof, E.C.: 1973, A coronal hole and its identification as the source of a high velocity solar wind stream. *Solar Phys.* **29**, 505. DOI. ADS.

Krista, L.D., Gallagher, P.T.: 2009, Automated coronal hole detection using local intensity thresholding techniques. *Solar Phys.* **256**, 87. DOI. ADS.

Landi, E., Alexander, R.L., Gruesbeck, J.R., Gilbert, J.A., Lepri, S.T., Manchester, W.B., Zurbuchen, T.H.: 2012a, Carbon ionization stages as a diagnostic of the solar wind. *Astrophys. J.* **744**, 100. DOI. ADS.

Landi, E., Gruesbeck, J.R., Lepri, S.T., Zurbuchen, T.H.: 2012b, New solar wind diagnostic using both in situ and spectroscopic measurements. *Astrophys. J.* **750**, 159. DOI. ADS.

Lepri, S.T., Landi, E., Zurbuchen, T.H.: 2013, Solar wind heavy ions over solar cycle 23: ACE/SWICS measurements. *Astrophys. J.* **768**, 94. DOI. ADS.

Levine, R.H.: 1982, Open magnetic fields and the solar cycle. I – Photospheric sources of open magnetic flux. *Solar Phys.* **79**, 203. DOI. ADS.

Li, B., Habbal, S.R., Li, X., Mountford, C.: 2005, Effect of the latitudinal distribution of temperature at the coronal base on the interplanetary magnetic field configuration and the solar wind flow. *J. Geophys. Res.* **110**, 12112. DOI. ADS.

Liewer, P.C., Neugebauer, M., Zurbuchen, T.: 2004, Characteristics of active-region sources of solar wind near solar maximum. *Solar Phys.* **223**, 209. DOI. ADS.

Luhmann, J.G., Li, Y., Arge, C.N., Gazis, P.R., Ulrich, R.: 2002, Solar cycle changes in coronal holes and space weather cycles. *J. Geophys. Res.* **107**, 1154. DOI. ADS.

Madjarska, M.S., Huang, Z., Doyle, J.G., Subramanian, S.: 2012, Coronal hole boundaries evolution at small scales. III. EIS and SUMER views. *Astron. Astrophys.* **545**, A67. DOI. ADS.

Mandrini, C.H., Nuevo, F.A., Vásquez, A.M., Démoulin, P., van Driel-Gesztelyi, L., Baker, D., Culhane, J.L., Cristiani, G.D., Pick, M.: 2014, How can active region plasma escape into the solar wind from below a closed helmet streamer? *Solar Phys.* **289**, 4151. DOI. ADS.

Marsch, E.: 2006, Kinetic physics of the solar corona and solar wind. *Living Rev. Solar Phys.* **3**, 1. DOI. ADS.

Mazzotta, P., Mazzitelli, G., Colafrancesco, S., Vittorio, N.: 1998, Ionization balance for optically thin plasmas: rate coefficients for all atoms and ions of the elements H to Ni. *Astron. Astrophys. Suppl.* **133**, 403. DOI. ADS.

McComas, D.J., Bame, S.J., Barker, P., Feldman, W.C., Phillips, J.L., Riley, P., Griffee, J.W.: 1998, Solar wind electron proton alpha monitor (SWEPAM) for the advanced composition explorer. *Space Sci. Rev.* **86**, 563. DOI. ADS.

Neugebauer, M., Forsyth, R.J., Galvin, A.B., Harvey, K.L., Hoeksema, J.T., Lazarus, A.J., Lepping, R.P., Linker, J.A., Mikic, Z., Steinberg, J.T., von Steiger, R., Wang, Y.-M., Wimmer-Schweingruber, R.F.: 1998, Spatial structure of the solar wind and comparisons with solar data and models. *J. Geophys. Res.* **103**, 14587. DOI. ADS.

Neugebauer, M., Liewer, P.C., Smith, E.J., Skoug, R.M., Zurbuchen, T.H.: 2002, Sources of the solar wind at solar activity maximum. *J. Geophys. Res.* **107**, 1488. DOI. ADS.

Noci, G., Kohl, J.L., Antonucci, E., Tondello, G., Huber, M.C.E., Fineschi, S., Gardner, L.D., Korendyke, C.M., Nicolosi, P., Romoli, M., Spadaro, D., Maccari, L., Raymond, J.C., Siegmund, O.H.W., Benna, C., Ciaravella, A., Giordano, S., Michels, J., Modigliani, A., Naletto, G., Panasyuk, A., Pernechele, C., Poletto, G., Smith, P.L., Strachan, L.: 1997, The quiescent corona and slow solar wind. In: Wilson, A. (ed.) *Fifth SOHO Workshop: The Corona and Solar Wind Near Minimum Activity*, *ESA* **SP-404**, 75. ADS.

Nolte, J.T., Roelof, E.C.: 1973, Large-scale structure of the interplanetary medium, I: High coronal source longitude of the quiet-time solar wind. *Solar Phys.* **33**, 241. DOI. ADS.

Owocki, S.P., Holzer, T.E., Hundhausen, A.J.: 1983, The solar wind ionization state as a coronal temperature diagnostic. *Astrophys. J.* **275**, 354. DOI. ADS.

Poletto, G.: 2013, Sources of solar wind over the solar activity cycle. *J. Adv. Res.* **4**, 215. DOI. ADS.

Richardson, I.G., Cane, H.V.: 2004, Identification of interplanetary coronal mass ejections at 1 AU using multiple solar wind plasma composition anomalies. *J. Geophys. Res.* **109**, 9104. DOI. ADS.

Riley, P., Linker, J.A., Mikić, Z., Lionello, R., Ledvina, S.A., Luhmann, J.G.: 2006, A comparison between global solar magnetohydrodynamic and potential field source surface model results. *Astrophys. J.* **653**, 1510. DOI. ADS.

Sakao, T., Kano, R., Narukage, N., Kotoku, J., Bando, T., DeLuca, E.E., Lundquist, L.L., Tsuneta, S., Harra, L.K., Katsukawa, Y., Kubo, M., Hara, H., Matsuzaki, K., Shimojo, M., Bookbinder, J.A., Golub, L.,

Korreck, K.E., Su, Y., Shibasaki, K., Shimizu, T., Nakatani, I.: 2007, Continuous plasma outflows from the edge of a solar active region as a possible source of solar wind. *Science* **318**, 1585. DOI. ADS.

Schatten, K.H., Wilcox, J.M., Ness, N.F.: 1969, A model of interplanetary and coronal magnetic fields. *Solar Phys.* **6**, 442. DOI. ADS.

Schrijver, C.J., De Rosa, M.L.: 2003, Photospheric and heliospheric magnetic fields. *Solar Phys.* **212**, 165. DOI. ADS.

Schwenn, R.: 2006, Solar wind sources and their variations over the solar cycle. *Space Sci. Rev.* **124**, 51. DOI. ADS.

Sheeley, N.R., Wang, Y.-M., Hawley, S.H., Brueckner, G.E., Dere, K.P., Howard, R.A., Koomen, M.J., Korendyke, C.M., Michels, D.J., Paswaters, S.E., Socker, D.G., St. Cyr, O.C., Wang, D., Lamy, P.L., Llebaria, A., Schwenn, R., Simnett, G.M., Plunkett, S., Biesecker, D.A.: 1997, Measurements of flow speeds in the corona between 2 and 30 $R_{\odot}$. *Astrophys. J.* **484**, 472. ADS.

Smith, C.W., L'Heureux, J., Ness, N.F., Acuña, M.H., Burlaga, L.F., Scheifele, J.: 1998, The ACE magnetic fields experiment. *Space Sci. Rev.* **86**, 613. DOI. ADS.

Snyder, C.W., Neugebauer, M.: 1966, The relation of Mariner-2 plasma data to solar phenomena. In: Mackin, R.J. Jr., Neugebauer, M. (eds.) *The Solar Wind*, 25. ADS.

Stone, E.C., Frandsen, A.M., Mewaldt, R.A., Christian, E.R., Margolies, D., Ormes, J.F., Snow, F.: 1998, The advanced composition explorer. *Space Sci. Rev.* **86**, 1. DOI. ADS.

Subramanian, S., Madjarska, M.S., Doyle, J.G.: 2010, Coronal hole boundaries evolution at small scales. II. XRT view. Can small-scale outflows at CHBs be a source of the slow solar wind. *Astron. Astrophys.* **516**, A50. DOI. ADS.

Suess, S.T., Wang, A.-H., Wu, S.T., Nerney, S.F.: 1999, Streamer evaporation. *Space Sci. Rev.* **87**, 323. DOI. ADS.

Tu, C.-Y., Zhou, C., Marsch, E., Xia, L.-D., Zhao, L., Wang, J.-X., Wilhelm, K.: 2005, Solar wind origin in coronal funnels. *Science* **308**, 519. DOI. ADS.

van Driel-Gesztelyi, L., Culhane, J.L., Baker, D., Démoulin, P., Mandrini, C.H., DeRosa, M.L., Rouillard, A.P., Opitz, A., Stenborg, G., Vourlidas, A., Brooks, D.H.: 2012, Magnetic topology of active regions and coronal holes: implications for coronal outflows and the solar wind. *Solar Phys.* **281**, 237. DOI. ADS.

Wang, Y.-M., Sheeley, N.R. Jr.: 1990, Solar wind speed and coronal flux-tube expansion. *Astrophys. J.* **355**, 726. DOI. ADS.

Wang, Y.-M., Sheeley, N.R. Jr.: 2003, The solar wind and its magnetic sources at sunspot maximum. *Astrophys. J.* **587**, 818. DOI. ADS.

Wang, Y.-M., Ko, Y.-K., Grappin, R.: 2009, Slow solar wind from open regions with strong low-coronal heating. *Astrophys. J.* **691**, 760. DOI. ADS.

Wang, Y.-M., Sheeley, N.R. Jr., Walters, J.H., Brueckner, G.E., Howard, R.A., Michels, D.J., Lamy, P.L., Schwenn, R., Simnett, G.M.: 1998, Origin of streamer material in the outer corona. *Astrophys. J. Lett.* **498**, L165. DOI. ADS.

Xia, L.D., Marsch, E., Curdt, W.: 2003, On the outflow in an equatorial coronal hole. *Astron. Astrophys.* **399**, L5. DOI. ADS.

Zhao, L., Landi, E.: 2014, Polar and equatorial coronal hole winds at solar minima: from the heliosphere to the inner corona. *Astrophys. J.* **781**, 110. DOI. ADS.

Zhao, L., Zurbuchen, T.H., Fisk, L.A.: 2009, Global distribution of the solar wind during solar cycle 23: ACE observations. *Geophys. Res. Lett.* **36**, 14104. DOI. ADS.

Zharkova, V.V., Aboudarham, J., Zharkov, S., Ipson, S.S., Benkhalil, A.K., Fuller, N.: 2005, Solar feature catalogues in EGSO. *Solar Phys.* **228**, 361. DOI. ADS.

Zirker, J.B.: 1977, Coronal holes and high-speed wind streams. *Rev. Geophys. Space Phys.* **15**, 257. DOI. ADS.

Zurbuchen, T.H.: 2001, Heliospheric magnetic field configuration and its coronal sources. In: Brekke, P., Fleck, B., Gurman, J.B. (eds.) *Recent Insights into the Physics of the Sun and Heliosphere: Highlights from SOHO and Other Space Missions*, *IAU Symposium* **203**, 585. ADS.

Zurbuchen, T.H., Hefti, S., Fisk, L.A., Gloeckler, G., Schwadron, N.A.: 2000, Magnetic structure of the slow solar wind: constraints from composition data. *J. Geophys. Res.* **105**, 18327. DOI. ADS.